



Studies on the Effect of Some Pyrimidine Derivatives on the Corrosion of Iron in 1M Hydrochloric Acid

K. M. Abdel-Azim*, M. Saleh, N. S. Abdelshafi, K. F. Khaled

Electrochemistry Research Laboratory, Chemistry Department, Faculty of Education, Ain Shams

University, Roxy, Cairo, Egypt.



CrossMark

Abstract

The effect of three pyrimidine derivatives namely, 6-amino-3,4-dihydropyrimidin-2(1H)-thione (Pyr-3), ethyl (R)-2-mercapto-4-methyl-6-phenyl-1,6-dihydropyrimidine-5-carboxylate (Pyr-7) and ethyl (R)-6-(4-chlorophenyl)-2-mercapto-4-methyl-1,6-dihydropyrimidine-5-carboxylate (Pyr-9) on the corrosion of iron in 1.0 M HCl in absence and presence of various concentrations ranging from 10^{-3} to 10^{-7} M has been studied. Both electrochemical (potentiodynamic, electrochemical impedance spectroscopy and electrochemical frequency modulation) and computational studies (quantum chemical calculations and molecular dynamic simulations) have been used in this study. Electrochemical investigations show the effectiveness of the studied pyrimidine derivatives as corrosion inhibitors. The best inhibition efficiency reached 96% for Pyr-9 at 10^{-3} M. The studied pyrimidine derivatives were of mixed type inhibitor. Equivalent circuit for the studied system was determined. The studied pyrimidine derivatives follow Langmuir adsorption isotherm. Computational study confirms the experimental investigation.

Keywords: Acid Corrosion Inhibition; EFM; EIS; Equivalent Circuit; Monte Carlo simulation.

1. Introduction

Using inhibitors is one of the most effective methods of combat corrosion [1]. Acid solutions have wide application in industry such as acid cleaning, acid descaling and acid pickling [2]. Acid corrosion inhibitors are generally contains heteroatoms as sulphur, oxygen and nitrogen to achieve high inhibition efficiency [3, 4]. There are several studies on the corrosion inhibition of iron and its alloys in acid media using organic inhibitors [5-7]. Pyrimidine is a heterocyclic aromatic organic compound similar to benzene and pyridine, containing two nitrogen atoms at positions 1 and 3 of the six-member ring [8]. Studies on pyrimidine are limited in spite of their ease of availability and corrosion inhibition properties. Analgesics, antipyretics, antihypertensive, anti-inflammatory medicines, poisons, herbicides, plant growth regulators, and herbal calcium channel modulators are only a few of the many uses for them in the pharmaceutical industry [9, 10].

Several investigations have been made on using pyrimidine derivatives as promising corrosion inhibitor candidates [6, 11, 12]. The inhibition achieved by pyrimidine derivatives have been

explained on the basis of molecular adsorption by controlling anodic as well as cathodic sites of the iron surface [13]. Several electrochemical techniques have been used to investigate the adsorption of pyrimidine derivatives on metal surface include potentiodynamic polarization as well as electrochemical impedance spectroscopy, EIS [14].

Computational investigations conducted on corrosion inhibition of iron in acid media using pyrimidine derivatives used quantum chemical calculations [6]. Theoretical investigations shows the role of frontier molecular orbitals in understanding the inhibition mechanism [15]. The aim of this study is to expand the knowledge about three new pyrimidine derivatives candidates, namely, 6-amino-3,4-dihydropyrimidin-2(1H)-thione (Pyr-3), ethyl (R)-2-mercapto-4-methyl-6-phenyl-1,6-dihydropyrimidine-5-carboxylate (Pyr-7) and ethyl (R)-6-(4-chlorophenyl)-2-mercapto-4-methyl-1,6-dihydropyrimidine-5-carboxylate (Pyr-9) using, in addition to potentiodynamic polarization and electrochemical impedance spectroscopy, the new electrochemical frequency modulation technique, EFM. Also, the objective of this study is to

*Corresponding author e-mail: khaledelectro72@gmail.com; (Khaled M. Abdel-Azim).

Receive Date: 09 March 2021, Revise Date: 12 March 2021, Accept Date: 28 March 2021

DOI: 10.21608/EJCHEM.2021.64425.3387

©2021 National Information and Documentation Center (NIDOC)

investigate the adsorption of pyrimidine derivatives candidates on the iron surface using molecular dynamic simulations.

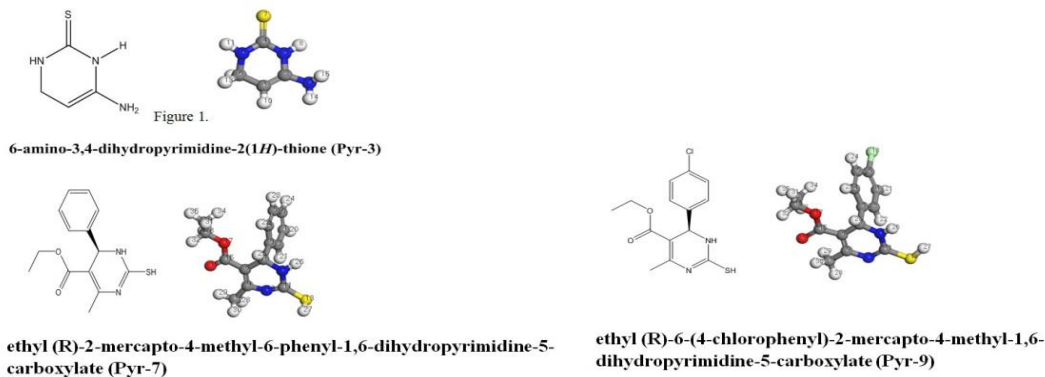


Fig.1. Chemical structures of the studied compound

2. Experimental

The pyrimidine derivatives investigated as possible corrosion inhibitors in hydrochloric acid are presented in figure 1. All pyrimidine derivatives namely, 6-amino-3,4-dihydropyrimidin-2(1*H*)-thione (Pyr-3), ethyl (R)-2-mercapto-4-methyl-6-phenyl-1,6-dihydropyrimidine-5-carboxylate (Pyr-7) and ethyl (R)-6-(4-chlorophenyl)-2-mercapto-4-methyl-1,6-dihydropyrimidine-5-carboxylate (Pyr-9) were prepared as described elsewhere [16-18]. The corrosive solution (1.0 M HCl) was prepared by dilution of analytical grade 37 % HCl solution with double-distilled water. Prior to each experiment cylindrical rods of iron (Puratronic 99.999%) were mounted in Teflon and filled with epoxy. The electrode with surface area (0.28 cm²) was polished with emery papers with different grit size up to 4/0, washed thoroughly with double-distilled water, degreased with acetone and drying at room temperature, 25 ± 1°C. A typical three electrode cell consisted of the iron sample as working electrode, platinum mesh as counter electrode, and a saturated calomel electrode as the reference electrode. The working electrode potential was stabilized by immersing the electrode for an hour prior to each

measurement. Measurements were performed using Gamry 3000 controlled by Gamry framework and Echem Analyst version 6.33. Potentiodynamic polarization curves were recorded by changing the electrode potential (-500 to +500 mV_{SCE}) at open circuit potential with scan rate of 0.005 V s⁻¹. The frequency range of the impedance measurements were from 100 kHz to 20. mHz with an amplitude of ±10 mV peak-to-peak using ac signals at open circuit potential. Electrochemical frequency modulation, EFM, was conducted using 2 Hz and 5 Hz frequencies. One Hz was the base frequency, so the waveform repeats after 1s.

3. Computational details

The molecular dynamics module in Materials Studio 7.0 software from BIOVIA [19] has been used to study the adsorption of pyrimidine derivatives candidates on the iron surface. The Metropolis Monte Carlo method [20] included in Adsorption Locator module [21, 22] is used to calculate the low energy configuration of the three inhibitor candidates Pyr-3, Pyr-7, and Pyr-9 on the iron surface. The molecular dynamics simulations procedures have been described elsewhere [23, 24].

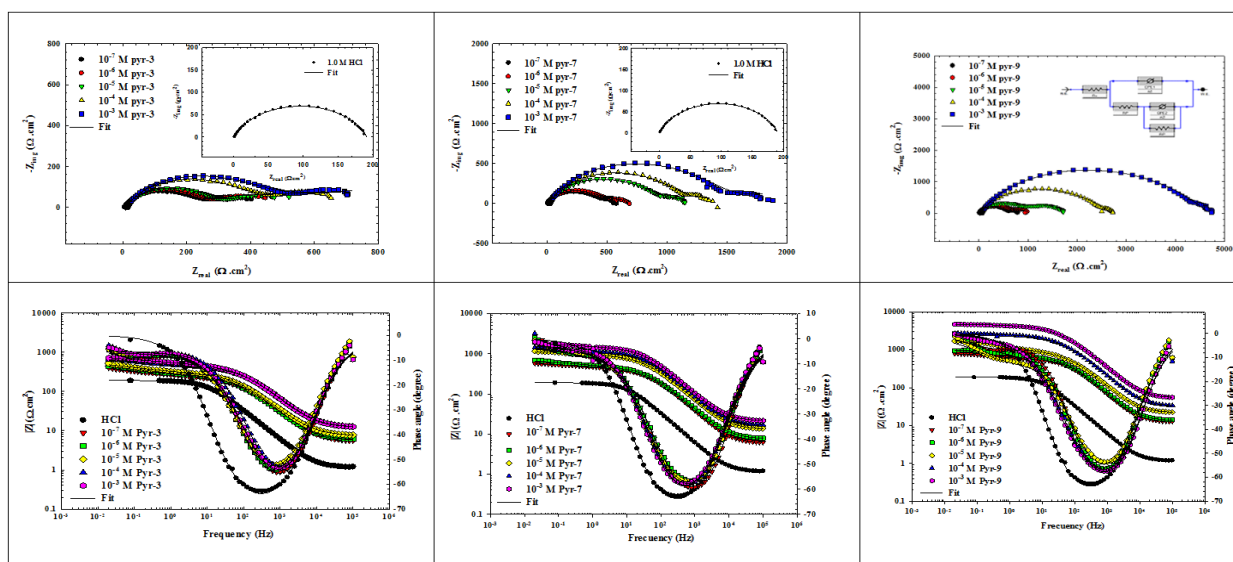


Fig.2. Nyquist plots, Bode plots and equivalent circuit for the studied Iron/Pyrimidine system in 1.0 M HCl at 25 ± 1°C

4. Results and discussions

4.1 Electrochemical Impedance Spectroscopy (EIS)

The Nyquist plots for the iron in 1.0 M HCl was characterized by one semi-circular but pyrimidine derivatives inhibited solutions were characterized by two semi-circular capacitive loops. Figure 2 shows Nyquist plots, which are depressed semi-circular curves with their centers under the real axis. Impurities on the electrode surface, electrode surface roughness and inhomogeneity, and inhibitor adsorption on the electrode surface all contribute to the imperfection in the semi-circular capacitive arc [25]. The diameter of the Nyquist plots for the inhibited solutions was clearly greater than the blank solution, and this diameter increased with increasing inhibitor concentration, peaking at 10⁻³M. It ensures that the corrosion is mediated by the pyrimidine derivatives (Pyr)s molecules adsorbing on the iron surface, forming a protective layer against the electrolyte corrosive species and thereby increasing the iron resistance to electrochemical corrosion [25, 26]. Pyrimidine derivatives molecules adsorbed on the iron surface through the formation of a coordinate covalent bond between the iron surface and the heteroatoms of pyrimidine derivatives molecules, forming a metal/pyrimidine derivatives complex film on the iron surface that effectively blocks acid attack. The impedance plots for the inhibited solutions are identical, indicating that the inhibitor reduces metal corrosion without altering the mechanism of corrosion [27]. The parameters from electrochemical impedance such as polarization resistance (R_p), heterogeneity (n), constant phase element (CPE) and solution resistance (R_s) were calculated by fitting the impedance spectra to the corresponding equivalent

circuit model shown in figure 2 and are presented in Table 1. The inhibition efficiency, $E_i\%$ of Pyr-3, Pyr-7 and Pyr-9 for the iron electrode can be calculated from the polarization resistance, R_p as follow: [28]

$$E_i \% = \left(1 - \frac{R_p^o}{R_p}\right) \times 100 \quad (1)$$

Where R_p^o and R_p are the polarization resistances in absence and presence of pyrimidine derivatives, respectively.

The two semi-circular capacitive corresponding to two time constants at high and low frequency regions in the Bode plots; where the time constant at the high frequency region represent a defective/porous protective pyrimidine derivatives film on the iron surface ($R_p // CPE_1$) while the time constant ($R'_p // CPE_2$) at the low frequency region represents the formation of a double layer at the metal/electrolyte interface [25]. Addition of Pyr-3, Pyr-7 and Pyr-9 increases the values of R_p and R'_p and this effect is seen to be increased as the concentrations of Pyr-3, Pyr-7 and Pyr-9 increase [29]. This is due to the formation of pyrimidine derivatives protective film on the iron surface, which blocks the iron surface from attack by the electrolyte corrosive species, thereby protecting the surface from further charge and mass transfer. The constant phase elements (CPEs) with their n values $1 > n > 0$ represent double layer capacitors with some pores [30]. Furthermore, the inhibited solutions had a higher value of solution resistance (R_s) than the blank solution, indicating that the inhibited solutions had less current flow and therefore had a lower corrosion

rate. The inhibition efficiency reaches a maximum value of 96% at 10^{-3} M for Pyr-9. The Pyr-9 compound is more adsorbent than all other compounds. The Bode diagrams of iron electrode in 1.0 M HCl in the absence and in the presence of the Pyr-3, Pyr-7 and Pyr-9 at various concentrations are shown in figure 2. As can be seen, it is clear that the phase angles are increased with increasing of the Pyr-3, Pyr-7 and Pyr-9 concentrations. This increase in phase angles confirms higher protection by increasing the concentration of Pyr-3, Pyr-7 and Pyr-9 [31]. From the bode diagrams we have noticed that there are three frequency domains: low, high and middle of

the road frequencies. At low frequencies there is a rise in absolute values of impedance that approve the greatest inhibition as the concentration of pyrimidine derivatives increases [32]. However at high frequency, the values absolute impedance and the phase shift are diminished (close to zero) which represent the solution resistance of the studied iron electrode. At the middle frequency region a linear relationship between $\log |Z|$ and frequency with a negative slope close to unity and the phase angle is close to 66° has been observed [32]. This shows that the capacitive behavior at intermediate frequencies.

Table.1. Electrochemical parameters obtained from EIS for Iron in 1M HCl without and with various concentrations of Pyr-3, Pyr-7 and Pyr-9 at 25 ± 1 °C.

Inhibitors	Conc. M	$R_s / \Omega\text{cm}^2$	$R_p / \Omega\text{cm}^2$	$CPE_1 \Omega^{-1}\text{cm}^{-2}\text{s}^{n_1} \times 10^6$	n_1	$R_p' / \Omega\text{cm}^2$	$CPE_2 \Omega^{-1}\text{cm}^{-2}\text{s}^{n_2} \times 10^6$	n_2	$E_i\%$
Pyr-3	Blank	1.1	189.8	165.5	0.80	-	-	-	-
	10^{-7}	5.50	260	100.5	0.08	144	51.2	0.82	53.0
	10^{-6}	5.77	287	88.59	0.43	155	37.51	0.77	57.0
	10^{-5}	7.29	314	76.8	0.44	214	31.6	0.09	64.0
	10^{-4}	12.23	420	63.5	0.28	235	29.0	0.79	71.0
	10^{-3}	12.17	440	24.9	0.12	264	23.2	0.80	73.0
Pyr-7	10^{-7}	5.92	466	68.4	0.24	128	22.3	0.83	68.0
	10^{-6}	7.38	506	61.5	0.39	198	20.1	0.78	73.0
	10^{-5}	12.83	947	53.5	0.12	241	15.7	0.79	84.0
	10^{-4}	16.25	1153	29.7	0.05	309	11.23	0.80	87.0
	10^{-3}	20.77	1500	11.3	0.10	400	9.66	0.79	90.0
Pyr-9	10^{-7}	12.02	610	56.3	0.61	182	13.22	0.80	76.0
	10^{-6}	13.25	728	50.1	0.53	222	12.91	0.80	80.0
	10^{-5}	21.39	1050	42.2	0.51	677	9.70	0.78	89.0
	10^{-4}	32.54	2000	19.7	0.43	714	4.3	0.82	93.0
	10^{-3}	54.24	3975	8.1	0.54	775	1.14	0.87	96.0

4.2 Electrochemical frequency modulation (EFM)

Electrochemical frequency modulation, EFM is a very powerful tool to determine the corrosion current without the need of knowledge of tafel slopes values. EFM is similar to impedance that both use small ac signal, but differ from EIS that, two sine waves (at different frequencies) are applied to the cell instantaneously. As the applied current is a non-linear function of potential, the corrosion system replies in a non-linear way to the applied wave. The response to

the excitation wave (the current response) has in addition to the input frequencies, it also, has frequency components that are addition, difference and multiplies of the two input frequencies [33]. An internal check for the validity of the EFM data is the causality factors [33, 34]. The intermodulation EFM spectra of the iron electrode immersed in 1.0 M HCl in the absence and in the presence of the different concentrations of Pyr-3, Pyr-7 and Pyr-9 depicted in figure 3.

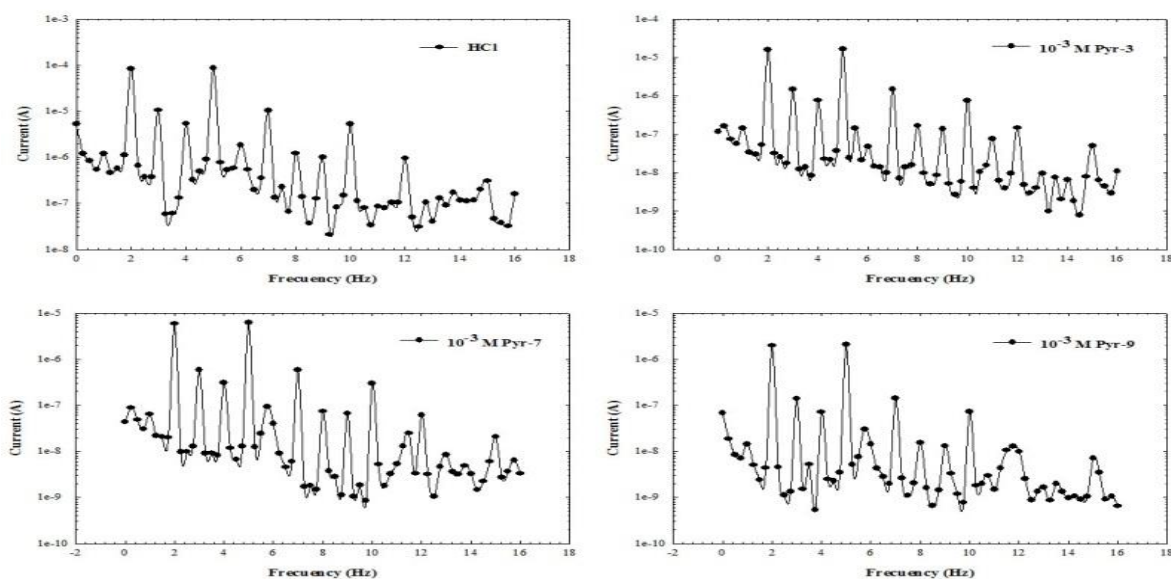


Fig.3. Intermodulation spectrum for Iron in 1.0 M HCl without and with 10^{-3} M of Pyr-3 at $25 \pm 1^\circ\text{C}$ (representative examples)

The electrochemical kinetic data calculated from the EFM spectra are given as follows: [35, 36]

$$i_{corr} = \frac{i_{\omega}^2}{\sqrt{48(2i_{\omega}i_{3\omega} - i_{2\omega}^2)}} \quad (2)$$

$$\beta_a = \frac{i_{\omega}U_o}{2i_{2\omega} + 2\sqrt{3}\sqrt{2i_{3\omega}i_{\omega} - i_{2\omega}^2}} \quad (3)$$

$$\beta_c = \frac{i_{\omega}U_o}{2\sqrt{3}\sqrt{2i_{3\omega}i_{\omega} - i_{2\omega}^2} - 2i_{2\omega}} \quad (4)$$

$$\text{Causality factor (2)} = \frac{i_{\omega 2 \pm \omega_1}}{i_{2\omega_1}} = 2.0 \quad (5)$$

$$\text{Causality factor (3)} = \frac{i_{2\omega_2 \pm \omega_1}}{i_{3\omega_1}} = 3.0 \quad (6)$$

where i is the instantaneous current density at the working electrode measured at frequency ω and U_0 is the amplitude of the sine wave distortion. The inhibition efficiency, $E_{EFM\%}$, of Pyr-3, Pyr-7 and Pyr-9 were calculated at different concentrations using equation presented below: [20]

$$E_{EFM} \% = \left(1 - \frac{i_{corr}}{i_{corr}^o}\right) \times 100 \quad (7)$$

Where i_{corr}^o and i_{corr} are corrosion current density in the absence and presence of Pyr-3, Pyr-7 and Pyr-9, respectively. The determined electrochemical parameters (i_{corr} , b_a , b_c , CF-2, CF-3 and $E_{EFM\%}$) are shown in table 2. As can be seen from table 2, the

corrosion current densities decrease with increase in Pyr-3, Pyr-7 and Pyr-9 concentrations.

The goodness of the EFM data is appeared from the acceptable values of the CF-2 and CF-3 which are close to 2.0 and 3.0, respectively. The values of the causality factors in the current study confirm the casual relation between the disturbance signal and the response signal [37]. In table 2, addition of increasing concentration of Pyr-3, Pyr-7 and Pyr-9 to 1.0 M HCl solutions decreases the corrosion current density (i_{corr}), indicating that Pyr-3, Pyr-7 and Pyr-9 inhibits the iron corrosion in 1.0 M HCl solutions through adsorption. The calculated inhibition efficiency $E_{EFM\%}$ increases with increasing of Pyr-3, Pyr-7 and Pyr-9 concentrations. The presence of Pyr-3, Pyr-7 and Pyr-9 decreases the corrosion current density at any given concentration indicating inhibition of the corrosion process. The inhibition function of these compounds is attributed to their adsorption on the surface of the iron electrode. The Tafel constants b_a and b_c do not change significantly with increasing the concentration of the Pyr-3, Pyr-7 and Pyr-9 confirming the assumption that these inhibitors do not change the mechanism of the corrosion reactions.

4.3 Potentiodynamic polarization measurements

Figure 4 shows the effect of Pyr-3, Pyr-7 and Pyr-9 on the polarization curves for iron rod immersed hydrochloric acid at $25^\circ\text{C} \pm 1$. Addition of Pyr-3, Pyr-7 and Pyr-9 move the cathodic Tafel lines to lower values of corrosion current densities that decreases corrosion rate, however, they move the

anodic tafel line to lower values that easily retard the corrosion process.

Table.2. Electrochemical kinetic parameters obtained by EFM technique for Iron in 1M HCl with various concentrations of Pyr-3, Pyr-7 and Pyr-9 at 25±1 °C.

Inhibitors	Conc.	i_{corr}	b_a	b_c	C.R	E_{EFM} %	CF-2	CF-3
	M	$\mu A.cm^{-2}$	$mV.dec^{-1}$	$mV.dec^{-1}$	mpy			
	blank	177.8	89.0	278.4	81.25		1.97	1.02
Pyr-3	10^{-7}	71.09	96.0	127.2	32.49	60.01	1.98	2.92
	10^{-6}	65.79	157.0	253.8	30.06	62.99	1.93	3.24
	10^{-5}	55.12	123.0	239.9	25.19	68.99	1.94	3.12
	10^{-4}	44.44	135.50	282.1	20.31	75.00	1.98	3.11
	10^{-3}	37.34	105.10	254.2	17.06	78.99	1.95	3.04
Pyr-7	10^{-7}	47.96	97.09	106.4	21.91	73.00	1.45	1.36
	10^{-6}	42.66	128.6	236.1	19.49	76.00	1.99	3.01
	10^{-5}	21.34	114.3	230.5	9.75	87.99	1.98	1.66
	10^{-4}	15.98	96.96	240.9	7.30	91.00	1.96	2.65
	10^{-3}	12.47	95.80	220.7	5.69	92.90	1.93	2.19
Pyr-9	10^{-7}	37.34	109.4	152.2	17.06	78.99	1.99	3.11
	10^{-6}	30.22	154.5	283.6	13.81	83.00	1.98	1.90
	10^{-5}	12.50	117.9	265.8	5.71	92.90	2.03	2.07
	10^{-4}	7.16	135.9	321.3	3.27	95.90	1.97	2.87
	10^{-3}	5.29	124.2	262.8	2.42	97.00	1.96	1.25

Figure 4 indicates that the hydrogen evolution reaction (cathodic reaction) is under activation control. Furthermore, the mechanism of the cathodic

reaction does not affect much by the presence of Pyr-3, Pyr-7 and Pyr-9, this attributed to the nearly parallel cathodic tafel lines [38].

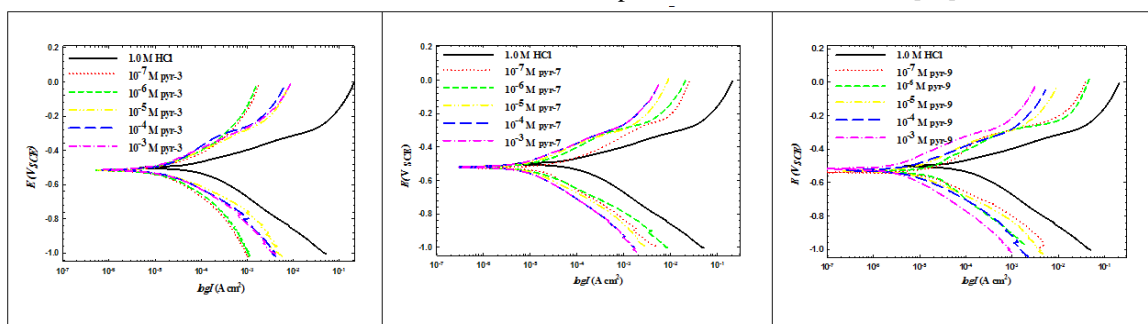


Fig.4. Anodic and cathodic potentiodynamic polarization curves for iron in 1.0 M HCl without and with different concentrations of pyrimidine derivatives at 25 ± 1 °C

Table 3 shows the electrochemical parameters extracted from potentiodynamic polarization curves in figure 4. Protection efficiency (μ %), Corrosion current densities (i_{corr}), cathodic Tafel slope (β_c), anodic Tafel slope (β_a) and corrosion potential (E_{corr}), are presented in table 3 as functions of Pyr-3, Pyr-7 and Pyr-9 concentrations. The protection efficiency (μ %) at various concentrations was calculated from the equation: [7]

$$\mu\% = \left(1 - \frac{i_{corr}}{i_{corr}^0}\right) \times 100 \quad (8)$$

where i_{corr} and i_{corr}^0 are corrosion current densities for iron in presence and absence of Pyr-3, Pyr-7 and Pyr-9. Corrosion current density in the presence of Pyr-3, Pyr-7 and Pyr-9, (i_{corr}) decreases as the

concentration of the inhibitors increase. Protection efficiency, (μ %) increases with the increase in the Pyr-3, Pyr-7 and Pyr-9 concentration. The increase in the protection efficiency (μ %) is attributed to the adsorption of Pyr-3, Pyr-7 and Pyr-9 molecules on iron /HCl interface. The maximum decrease in (i_{corr}) value was ($4.01 \mu A cm^{-2}$) with inhibition efficiency (μ %) (95.03) at concentration $10^{-3}M$ of the synthesized Pyr-9. Corrosion potential (E_{corr}) Values in the presence of Pyr-3, Pyr-7 and Pyr-9 has definite trend, at high inhibitor concentrations it shifts to positive direction. These observations propose that the studied Pyr-3, Pyr-7 and Pyr-9 can be described as of mixed-type with mainly anodic process [39].

Table .3. Electrochemical kinetic parameters obtained by Potentiodynamic polarization technique for Iron in 1.0M HCl without and with various concentrations of Pyr-3, Pyr-7 and Pyr-9 at 25 ±1°C.

Inhibitors	Conc.M	i_{corr} $\mu\text{A.cm}^{-2}$	$-E_{corr}$ mv	ba V.dec-1	bc V.dec-1	C.R mpy	μ %
		Blank	81.40	500	92.60	174.1	37.18
PYR-3	10^{-7}	39.80	518	272.2	339.9	18.19	51.10
	10^{-6}	36.60	516	275.4	312.4	16.71	55.03
	10^{-5}	30.90	516	188.7	207.5	14.11	62.03
	10^{-4}	26.00	515	193.2	210.6	11.86	68.05
	10^{-3}	23.60	512	181.6	209.2	10.77	71.00
PYR-7	10^{-7}	26.90	526	123.5	207.0	12.30	66.95
	10^{-6}	23.20	525	147.3	167.9	10.61	71.49
	10^{-5}	15.40	520	140.7	166.2	7.02	81.08
	10^{-4}	12.20	518	138.2	189.0	5.58	85.01
	10^{-3}	9.71	519	136.4	208.1	4.43	88.07
PYR-9	10^{-7}	20.30	540	182.9	160.5	9.27	75.06
	10^{-6}	17.10	535	151.9	210.4	7.83	78.99
	10^{-5}	9.70	530	141.4	171.9	4.43	88.08
	10^{-4}	8.10	527	130.1	198.6	3.73	89.96
	10^{-3}	4.01	518	151.4	196.7	1.84	95.03

4.4 Quantum chemical studies

Quantum chemical descriptors were calculated in table 4 to explain the electronic properties of Pyr-3, Pyr-7, and Pyr-9. The calculated HOMO and LUMO plots for Pyr-3, Pyr-7, and Pyr-9 are shown in figure 5.

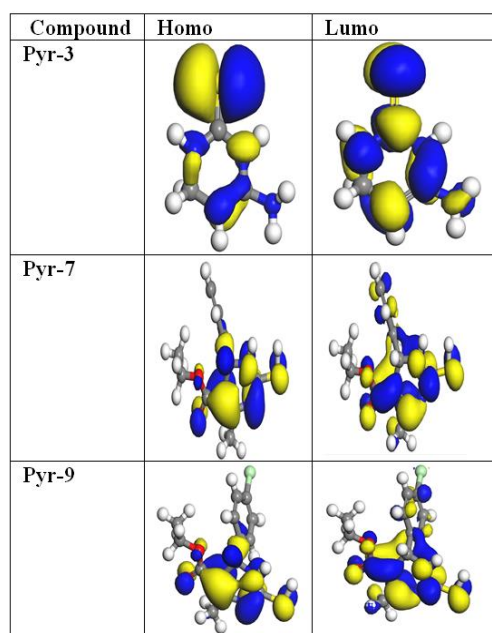


Fig. 5. HOMO and LUMO distributions for inhibitors Pyr-3, Pyr-7 and Pyr-9.

While only the calculated higher occupied molecular orbital, HOMO and lower unoccupied molecular orbital, LUMO and the difference between them, ΔE gap ($\Delta E = E_{LUMO} - E_{HOMO}$) are shown in Table 4 for shortness, several quantum chemical parameters are

included in table 4, for more additional molecular information. In the molecular orbital theory, HOMO/LUMO orbital, is a measure of the tendency of the molecule to donate /receive electrons. High HOMO values displays a higher tendency of the molecule to donate electrons that mean stronger adsorption on the metal surface and high inhibition efficiency [40, 41]. On the other side, a lower LUMO values displays that the molecule can receive electrons easily from the metal surface that mean better adsorption. Moreover, ΔE gap measures the reactivity of the molecule to be adsorbed on the iron surface [42]. Usually, as ΔE gap decreases the reactivity of the molecule increases that enhance inhibition efficiency of the inhibitor [40]. The values of our calculated HOMO, LUMO and LUMO-HOMO gaps, as introduced in Table 4, give that the order of inhibition efficiency is Pyr-9 > Pyr-7 > Pyr-3 in identical with the practical results. The HOMO values for all the three molecules are close to one another, the LUMO for Pyr-3 is higher compared to Pyr-7 and Pyr-9.

Moreover, E_{HOMO} and E_{LUMO} are correlated to the ionization potential (I) and the electron affinity (Y), respectively, are calculated from the following equations:[7]

$$I = -E_{HOMO} \quad (9)$$

$$Y = -E_{LUMO} \quad (10)$$

Then absolute electronegativity (ϕ), global hardness (ψ) and global softness (S) of the inhibitor molecule are calculated from the following equations: [7]

$$\phi = \frac{I+Y}{2} \quad (11)$$

$$\psi = \frac{I-Y}{2} \quad (12)$$

$$S = \frac{1}{\psi} \quad (13)$$

The number of electrons transported from inhibitor to metal surface (ΔN) is calculated depending on the quantum chemical method.

$$\Delta N = \frac{\phi_{\text{Fe}} - \phi_{\text{inh}}}{2(\psi_{\text{Fe}} + \psi_{\text{inh}})} \quad (14)$$

For pure iron, the theoretical values of ϕ_{Fe} and ψ_{Fe} are 7 eV and 0 eV, respectively [43, 44].

The values of ϕ , ψ , s and ΔN are also listed in table 4.

Table 4. Different quantum chemistry descriptors of Pyr-3, Pyr-7 and Pyr-9.

Inhibitors	E_{HOMO} eV	E_{LUMO} eV	ΔE eV	ϕ eV	ψ eV	s eV ⁻¹	ΔN
Pyr-3	-5.45	-1.31	4.14	3.38	2.0	0.48	0.905
Pyr-7	-5.33	-2.40	2.93	3.86	1.46	0.68	1.075
Pyr-9	-5.18	-2.57	2.61	3.87	1.30	0.76	1.203

According to literature [45], the parameter of ϕ is linked to the chemical potential, and higher estimation of ϕ implies better inhibitive performance. On the other hand, lower ψ implies more polarizability and bigger inhibition efficiency. The parameter of S is inverse ψ , thus great value of S lead to more efficiency. ΔN value less than 3.6 this

indicates that the inhibitor molecules have strong tendency to give electron to the vacant d-orbital of iron [46]. As can be seen the inhibitive action of Pyr-9 is higher than both Pyr-7 and Pyr-3 due to higher values of ϕ and s and lower values of ψ and ΔE .

Table 5. Calculated Fukui functions for the studied neutral inhibitor molecules.

Atoms	Pyr-3			Atoms	Pyr-7			Atoms	Pyr-9		
	f_k^+	f_k^-	Δf_k		f_k^+	f_k^-	Δf_k		f_k^+	f_k^-	Δf_k
C1	0.064	0.094	-0.03	C1	0.012	0.005	0.007	C1	0.013	0.011	0.002
C2	0.065	-0.016	0.081	C2	-0.011	-0.009	-0.002	C2	-0.005	-0.008	0.003
N3	0.011	0.013	-0.002	C3	-0.012	-0.004	-0.008	C3	-0.009	-0.005	-0.004
C4	0.083	0.023	0.060	C4	0.017	-0.006	0.023	C4	0.012	0.001	0.011
N5	0.046	0.007	0.039	C5	0.004	0.006	-0.002	C5	0.011	0.008	0.003
C6	-0.037	-0.026	-0.011	C6	0.018	0.011	0.007	C6	0.012	0.003	0.009
S7	0.326	0.476	-0.15	C7	-0.014	-0.029	0.015	C7	-0.009	-0.029	0.02
N9	0.018	0.039	-0.021	C8	0.038	0.104	-0.066	C8	0.038	0.100	-0.062
				C9	0.070	0.022	0.048	C9	0.070	0.023	0.047
				N10	0.034	0.099	-0.065	N10	0.043	0.086	-0.043
				C11	0.060	0.003	0.057	C11	0.048	0.006	0.042
				N12	0.032	0.052	-0.02	N12	0.025	0.056	-0.031
				S13	0.140	0.139	0.001	S13	0.131	0.144	-0.013
				C14	-0.022	-0.013	-0.009	C14	-0.021	-0.013	-0.008
				C15	0.054	0.029	0.025	C15	0.048	0.030	0.018
				O16	0.072	0.077	-0.005	O16	0.069	0.075	-0.006
				O17	0.021	0.016	0.005	O17	0.014	0.019	-0.005
				C18	-0.023	-0.021	-0.002	C18	0.075	0.068	0.007
				C19	-0.007	-0.011	0.004	C19	-0.022	-0.021	-0.001
								C20	-0.012	-0.008	-0.004

Fukui indices offer wealth of data about the nucleophilic and electrophilic practices just as the reactive areas of molecules. When the Fukui function is bigger the molecule areas are chemically softer. The Fukui function $f(\vec{r})$ is the first derived of the electronic density $p(\vec{r})$ as for the number of electrons N , in a constant external potential $v(\vec{r})$ and composed as follows: [41]

$$f(\vec{r}) = \left(\frac{\partial p(\vec{r})}{\partial N} \right)_{v(\vec{r})} \quad (15)$$

The nucleophilic attack Fukui function (f_k^+) and electrophilic attack Fukui function (f_k^-) can be calculated as [47, 48].

$$f_k^+ = q_i(N+1) - q_i(N) \quad (16)$$

$$f_k^- = q_i(N) - q_i(N-1) \quad (17)$$

Milliken atomic charge has been taken into account for this calculation [47, 48], where $q_i(N+1)$, $q_i(N)$, $q_i(N-1)$ are charge values of atom i for cation, neutral and anion, respectively. The N represents the number of electrons in the studied molecule, adding an electron to the LUMO of the neutral molecule gives $N+1$ (anion) and removing an electron from the neutral molecule gives $N-1$ (cation). The favored place for nucleophilic attack is the atom (or region) in the molecule where f_k^+ has the highest value while the place for electrophilic attack is the atom (or region) in the molecule where the value of f_k^- is the highest [49] Morell et al. [50, 51] have recently suggested a dual descriptor Δf_k , which is determined

as the difference between the nucleophilic and electrophilic Fukui functions and is given by

$$\Delta f_k = f_k^+ - f_k^- \quad (18)$$

When $\Delta f_k > 0$, then the site is favored for a nucleophilic attack, whereas if $\Delta f_k < 0$, then the site may be favored for an electrophilic attack [49]. The calculated Fukui function for the atoms compounds studied without hydrogen atoms, are presented in table 5. The favored site for electrophilic attack (shown by the highest value of f_k^- and the more negative value of Δf_k would first occur at C1, S7 and N9 in Pyr-3, at C8, N10 a, N12 and O16 in Pyr-7, at C8, N10, N12, S13, and O16 in Pyr-9. The favored site for nucleophilic attack (shown by the highest value of f_k^+ and Δf_k would first occur at C2, and C4 in Pyr-3, at C9, C11 and C15 in Pyr-7, at C9, C11 and C15 in Pyr-9.

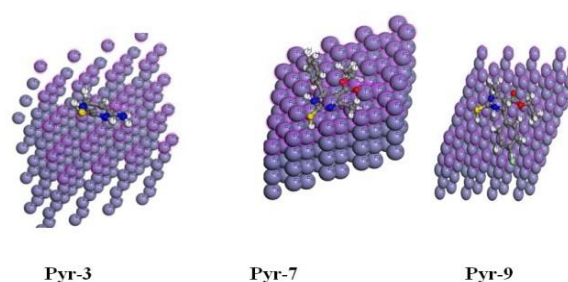


Fig. 6. Most suitable configuration for adsorption of Pyr-3, Pyr-7 and Pyr-9 on Fe (111) substrate obtained by adsorption locator module.

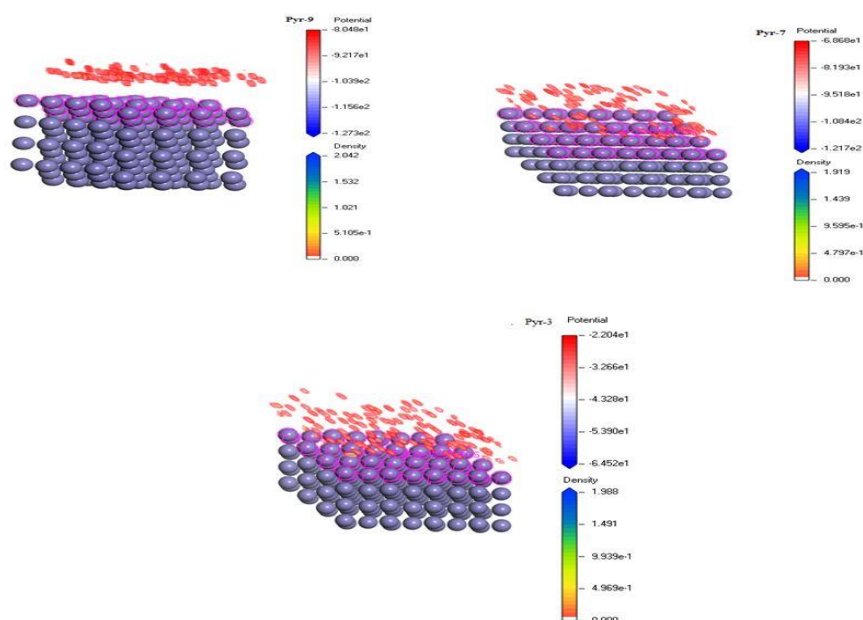


Fig. 7. The adsorption density of Pyr-3, Pyr-7 and Pyr-9 on the Iron surface substrate.

4.5 Molecular dynamic simulations

The Monte Carlo simulation (MD) method in adsorption studies makes an ensemble by suggesting a chain of configurations for the system under investigation [20]. It used to find centers of adsorption which have lowest energy on iron surfaces [52]. In this study, molecular dynamics techniques

are applied on a system comprising pyrimidine derivative and iron surface. Pyrimidine derivatives are relaxed on Fe surface, optimized and then (MD) performed, figure 6 and figure 8 show that the pyrimidine derivatives are adsorbed on iron surface and form a stable adsorption layer inhibit iron corrosion. Figure 7 shows the adsorption density of pyrimidine derivatives on the Fe surface.

Table .6. Output and descriptors calculated Monte Carlo simulation of Pyr-9, Pyr-7, and Pyr-3 confirmations on iron (111) surface.

Inhibitors	Total energy	Adsorption energy	Rigid adsorption energy	Deformation energy	dE_{ads}/dN_i
Pyr-9	-231.37	-127.25	-139.20	11.95	-127.25
Pyr-7	-225.74	-121.68	-127.53	5.85	-121.68
PYr-3	-224.76	-64.51	-65.99	1.47	-64.51

Parameters presented in table 6 show the calculated descriptors by the Monte Carlo simulation. These contain first total energy of the pyrimidine derivatives /iron surface and defined as the sum of the energies of the adsorbate pyrimidine derivatives, second, the rigid adsorption energy and third, the deformation energy. Adsorption energy expresses energy released (or required) when the relaxed pyrimidine derivatives are adsorbed on the iron surface [32]. The adsorption energy for the adsorbed inhibitor molecules is described as the sum of both the rigid adsorption energy and the deformation energy for these inhibitor molecules. Rigid adsorption energy reveals the energy released (or required) when the unrelaxed pyrimidine derivatives are adsorbed. Deformation energy reports the energy released when the pyrimidine derivatives are relaxed on surface [32]. (dE_{ads}/dN_i) , presented in table 6 reports the energy of iron/ pyrimidine derivatives configurations where one of the pyrimidine derivatives has been removed. Adsorption energy of the pyrimidine derivatives on iron surface are investigated and presented in Table 6 and Figure 8. The large negative value for adsorption energies in table 6 suggests that the inhibitor molecule strongly adsorbs onto the Fe (111) surface [53, 54]. The

adsorption energy of pyrimidine derivatives on iron surfaces, Table 6, confirmed the adsorption of Pyr-9 stronger than the other pyrimidine derivatives. Table 6 shows that Pyr-9 possesses the highest adsorption energy on Fe (111) surface, suggesting that Pyr-9 is the best inhibitor among the examined candidates. High values of adsorption energy support the experimental result.

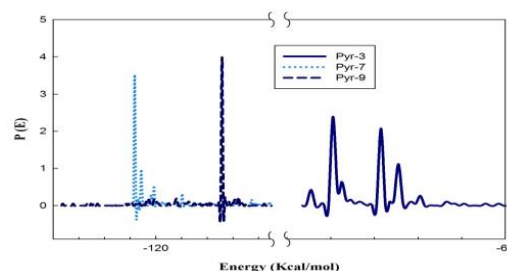


Fig.8. Adsorption energy distribution of the adsorbate Pyr-3, Pyr-7 and Pyr-9 on Iron surface.

Moreover, the radial distribution function (RDF) (or pair correlation function) $g(r)$ can be calculated after this analysis, figure 9.

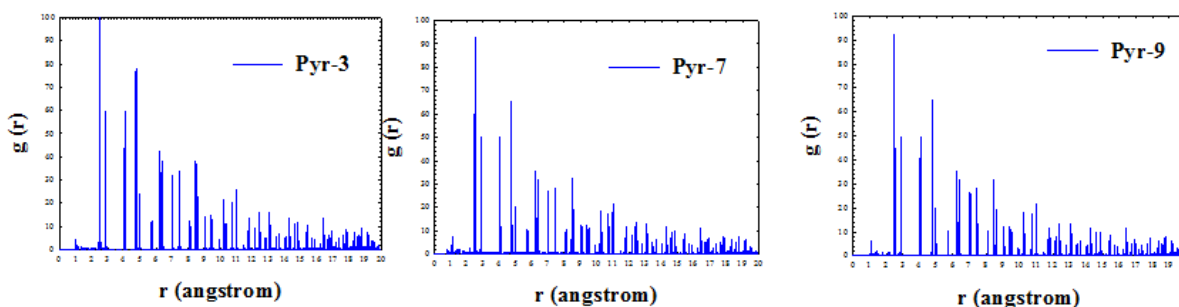


Fig.9. Radial distribution function of the Pyr-3, Pyr-7 and Pyr-9 on the Fe (111) surface in solution.

The RDF is utilized as an appropriate method to estimate the length of the link. The peak arises from 1 Å up to 3.5 Å; it is a sign of the length of small bonds, which is associated with chemisorption figure 9. While physisorption are associated with peaks greater than 3.5 Å. Moreover, the RDF of Pyr-3, Pyr-7 and Pyr-9 atoms displays that the bond length of iron is less than 3.5 Å the inhibitors is chemisorbed on Fe surface (figure 9) [55, 56].

4.6 Adsorption isotherm

The adsorption isotherms are utilized to describe the interaction of inhibitor particles with metal surfaces [57]. According to this isotherm, θ is related to the inhibitor concentration by the following equation.

$$\frac{C}{\theta} = \frac{1}{K_{ads}} + C \quad (19)$$

Where θ is the surface coverage, C is the concentration, K_{ads} is the equilibrium constant of adsorption process. K_{ads} is connected to the standard Gibbs free energy of adsorption ΔG_{ads}° by the equation (20). The information was acquired from figure 10. The intercept of the lines in these produced K_{ads} in M^{-1} , and the corresponding standard Gibbs free energy of adsorption in ($kJ mol^{-1}$) was then determined from equation (20).

$$\Delta G_{ads}^{\circ} = -RT \ln(55.5 K_{ads}) \quad (20)$$

where R in ($J mol^{-1} K^{-1}$) is the gas constant, T (K) is the temperature, and 55.5 denotes the concentration of water in $mol L^{-1}$

Table 7. Inhibitor binding constant (K_{ads}), Free energy of adsorption (ΔG_{ads}° , kJ/mol), for Pyr-3, Pyr-7 and Pyr-9 in in 1M HCl at $25 \pm 1^{\circ}C$, using potentiodynamic polarization measurements.

Inhibitor	ΔG_{ads}° ($kJ mol^{-1}$)	K_{ads} (M^{-1})
Pyr-3	-42.1	462320.8
Pyr-7	44.7	1263264.275
Pyr-9	-46.1	2222716.159

Using this equation 20, various adsorption parameters are calculated from the studied isotherm including the standard Gibbs free energy of adsorption of Pyr-3, Pyr-7 and Pyr-9 on the iron surface at $25 \pm 1^{\circ}C$ and listed in table 7. Figure 10 shows the adsorption isotherm for the studied pyrimidine derivatives. It follows from figure 10 that the studied candidates follows Langumir adsorption isotherm A linear relationship with $R^2 = 1$ are given and prove the Langumir adsorption isotherm model.

This adsorption model expect that the solid surface contains affixed number of adsorption sites, and each site joined to one adsorbed species [58] as well as no

interactions occur between the same species [59] and K_{ads} values increases with increasing inhibitor concentration showing that the molecules of the inhibitors were adsorbed on the iron surface and the adsorption process is more positive than desorption [59, 60].

The calculated values of ΔG_{ads}° , using Eq (20) are -42.1 kJ/mol, -44.7 kJ/mol and -46.1 kJ/mol for Pyr-3, Pyr-7 and Pyr-9 respectively. The large negative value of ΔG_{ads}° shows strong interactions between the inhibitor molecules and the iron surface [61, 62]. When the absolute value of ΔG_{ads}° is -40 kJ/mol or higher, the adsorption is viewed as chemisorption. When the absolute value of ΔG_{ads}° is -20 kJ/mol or lower, the adsorption is viewed as physisorption [63, 64]. In our case the inhibitors is chemisorbed on iron surface.

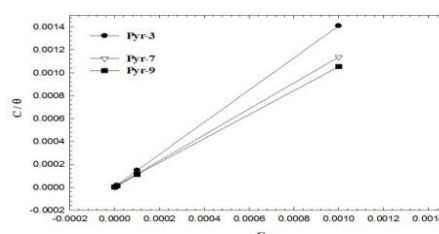


Fig.10. Langmuir adsorption isotherm of Iron in 1.0M HCl containing Pyr-3, Pyr-7 and Pyr-9 at $25 \pm 1^{\circ}C$.

4.7 Mechanism of adsorption

It is necessary to elucidate the corrosion inhibition mechanism of researched Pyr-3, Pyr-7 and Pyr-9. In 1.0 M HCl solutions, the final surface charge of iron electrode is negative, due to the presence of Cl^{-} anions that first adsorbed on the positively charged iron surface. Since chloride ions Cl^{-} have a smaller degree of hydration, being specifically adsorbed, they create an excess negative charge toward the solution and favor more adsorption of the cations. Pyr-3, Pyr-7 and Pyr-9 are organic compounds that can be adsorbed on the iron surface by several possible mechanisms. One of the suggested modes is the formation of coordinated bond between the vacant d-orbital in iron metal and the free lone pairs from N atom on the Pyr-3, Pyr-7 and Pyr-9. Other possible mechanisms involve the electrostatic attraction between the protonated Pyrs and $Fe(II)$ and form a dense and protective $[FeCl^{-}InhH^{+}]$ complex. Ultimately, the corrosive ions were blocked by the protective film and thus Fe was successfully protected.

5. Conclusion

In this study, three new pyrimidine derivatives were studied as possible inhibitors for corrosion of iron in 1.0 M HCl. Effectiveness of the studied pyrimidine derivatives were confirmed by both electrochemical methods and computational tools. Pyr-9 has the highest efficiency. Potentiodynamic polarization indicates that these inhibitors are of mixed type inhibitor. Equivalent circuit that described the studied system has two-time constants. Computational studies simulate the adsorption of these molecules on the iron surface. The adsorption of pyrimidine derivatives on the metal surface obeys Langmuir adsorption isotherm. Quantum chemical calculations showed that the calculated parameters correlated with experimental results.

6. Conflicts of interest

There are no conflicts to declare.

References

- [1] Z. Zhang, H. Ba, Z. Wu, Y. Zhu, The inhibition mechanism of maize gluten meal extract as green inhibitor for steel in concrete via experimental and theoretical elucidation, *Constr Build Mater.* 198 (2019) 288-298.
- [2] C. Wang, J. Chen, J. Han, C. Wang, B. Hu, Enhanced corrosion inhibition performance of novel modified polyaspartic acid on carbon steel in HCl solution, *J. Alloys Compd.* 771 (2019) 736-746.
- [3] H.L.Y. Sin, A. Al-Shishani, A. Abdul Rahim, B. Saad, B.R. Pandian, Corrosion inhibition potential of *Aquilaria* leaf constituents – A HPLC view, *Prog. Org. Coat.* 135(1) (2019) 536-544.
- [4] A.M. El-Shamy, M.F. Shehata, S.T. Gaballah, E.A. Elhefny, Synthesis and evaluation of ethyl (4-(n-(thiazol-2-yl) sulfamoyl) phenyl) carbamate (tspc) as a corrosion inhibitor for mild steel in 0.1M HCl, *Adv.Chem.* 11(2) (2015) 3441.
- [5] M.S. Ali, M.K. Emrana, M. Messalia, Improved protection performance of modified sol-gel coatings with pyridinium-based ionic liquid for cast iron corrosion in 0.5 M HCl solution, *Prog. Org. Coat.* 130(1) (2019) 226-234.
- [6] Z. Hajiahmadi, Z. Tavangar, Extensive theoretical study of corrosion inhibition efficiency of some pyrimidine derivatives on iron and the proposal of new inhibitor, *J. Mol. Liq.* 284 (2019) 225-231.
- [7] S.S. Abdel-Rehim, K.F. Khaled, N.A. Al-Mobarak, Corrosion inhibition of iron in hydrochloric acid using pyrazole, *Arab. J. Chem.* 4(3) (2011) 333-337.
- [8] A.S. Karpov, T.J. Mueller, Straightforward Novel One-Pot Enaminone and Pyrimidine Syntheses by Coupling-Addition-Cyclocondensation Sequences, *Synthesis* 18 (2003) 2815-2826.
- [9] N.A. Hassan, Syntheses of Furo[3,2-e][1,2,4]triazolo[1,5-c]pyrimidines and Furo[2',3':5,6]-pyrimido[3,4-b][2,3-e]indolo[1,2,4]triazine as a New Ring System, *Molecules* 5(6) (2000) 826-834.
- [10] C. Shishoo, K. Jain, Synthesis of some novel azido/tetrazolothienopyrimidines and their reduction to 2, 4-diaminothiemo [2, 3-d] pyrimidines, *J. Heterocycl. Chem.* 29(4) (1992) 883-893.
- [11] R. Yildiz, Adsorption and inhibition effect of 2,4-diamino-6-hydroxypyrimidine for mild steel corrosion in HCl medium: experimental and theoretical investigation, *Ionics* 25(2) (2018) 859-870.
- [12] I.R. Saad, A.M. Abdel-Gaber, G.O. Younes, B. Nsouli, Corrosion Inhibition of Mild Steel in Acidic Solutions Using 1,2,4-Triazolo[1,5-a]pyrimidine, *Russ. J. Appl. Chem.* 91(2) (2018) 245-252.
- [13] K.F. Khaled, Modeling corrosion inhibition of iron in acid medium by genetic function approximation method: A QSAR model, *Corros. Sci.* 53(11) (2011) 3457-3465.
- [14] D.K. Yadav, B. Maiti, M.A. Quraishi, Electrochemical and quantum chemical studies of 3,4-dihydropyrimidin-2(1H)-ones as corrosion inhibitors for mild steel in hydrochloric acid solution, *Corros. Sci.* 52(11) (2010) 3586-3598.
- [15] W. Zhang, H. Li, Y. Wu, Q. Luo, H. Liu, L. Niu, Adsorption Activity and Molecular Dynamics Study on Anti-corrosion Mechanism of Q235 Steel, *Chem. Res. Chin. Univ* 34(5) (2018) 817-822.
- [16] E.C. Taylor, C.C. Cheng, *J. Org. Chem* 25 (1960) 148-149.
- [17] K. Folkers, T. Johnson, *J. Am. Chem. Soc* 55 (1933) 2886-2893.
- [18] S.M. Sherif, M.M. Youssef, K.M. Mobarak, A.-S.M. Abdel-Fattah, A convenient synthesis of thiazolopyrimidines, thiazolodipyrimidines and heterocyclothiazolopyrimidines, *Tetrahedron* 49(42) (1993) 9561-9572.
- [19] J. Barriga, B. Coto, B. Fernandez, , *accelyrs, Tribol. Int.* 40 (2007) 960.
- [20] A.W.R. N. Metropolis, M.N. Rosenbluth, A.H. Teller, E. Teller, Equation of state calculations by fast computing machines, , *J. Chem. Phys.* 21 (1953) 1087-1092.
- [21] D. Frenkel, B. Smit, M.A. Ratner, *Understanding Molecular Simulation: From Algorithms to Applications* Academic Press, Calif, 1996.
- [22] S. Kirkpatrick, C.D. Gelatt, M.P. Vecchi,

- Optimization by simulated annealing, *Science* 220(1) (1983) 671-680.
- [23] N.A. Al-Mobarak, K.F. Khaled, M.N.H. Hamed, K.M. Abdel-Azim, N.S. Abdelshafi, Corrosion inhibition of copper in chloride media by 2-mercapto-4-(p-methoxyphenyl)-6-oxo-1,6-dihydropyrimidine-5-carbonitrile: Electrochemical and theoretical study, *Arab. J. Chem.* 3 (2010) 233-242.
- [24] B.S. Hou, Q.H. Zhang, Y.Y. Li, G.Y. Zhu, Y. Lei, X. Wang, H.F. Liu, G.A. Zhang, In-depth insight into the inhibition mechanism of pyrimidine derivatives on the corrosion of carbon steel in CO₂-containing environment based on experiments and theoretical calculations, *Corros. Sci.* 181(1) (2021) 109236.
- [25] K. Haruna, T.A. Saleh, M.A. Quraishi, Expired metformin drug as green corrosion inhibitor for simulated oil/gas well acidizing environment, *J. Mol. Liq.* 315 (2020) 113716.
- [26] F. Benhiba, H. Serrar, R. Hsissou, A. Guenbour, A. Bellaouchou, M. Tabyaoui, S. Boukhris, H. Oudda, I. Warad, A. Zarrouk, Tetrahydropyrimido-Triazepine derivatives as anti-corrosion additives for acid corrosion: Chemical, electrochemical, surface and theoretical studies, *Chem. Phys. Lett.* 743 (2020) 137181.
- [27] P. Dohare, M.A. Quraishi, I.B. Obot, A combined electrochemical and theoretical study of pyridine-based Schiff bases as novel corrosion inhibitors for mild steel in hydrochloric acid medium, *J Chem Sci* 8 (2018) 130-136.
- [28] W. Gong, X. Yin, Y. Liu, Y. Chen, W. Yang, 2-Amino-4-(4-methoxyphenyl)-thiazole as a novel corrosion inhibitor for mild steel in acidic medium, *Prog. Org. Coat.* 126(1) (2019) 150-161.
- [29] E.-S.M. Sherif, A.T. Abbas, D. Gopi, A.M. El-Shamy, Corrosion and Corrosion Inhibition of High Strength Low Alloy Steel in 2.0 M Sulfuric Acid Solutions by 3-Amino-1,2,3-triazole as a Corrosion Inhibitor, *Journal of Chemistry* 2014 (2014) 538794.
- [30] E.M. Sherif, S.-M. Park, 2-Amino-5-ethyl-1,3,4-thiadiazole as a corrosion inhibitor for copper in 3.0% NaCl solutions, *Corros. Sci.* 48(12) (2006) 4065-4079.
- [31] A. Yurt, S. Ulutas, H. Dal, Electrochemical and theoretical investigation on the corrosion of aluminium in acidic solution containing some Schiff bases, *Appl. Surf. Sci.* 253 (1) (2006) 919-925.
- [32] R. Hsissou, S. About, A. Berisha, M. Berradi, M. Assouag, N. Hajjaji, A. Elharfi, Experimental, DFT and molecular dynamics simulation on the inhibition performance of the DGDCBA epoxy polymer against the corrosion of the E24 carbon steel in 1.0 M HCl solution, *J. Mol. Struct.* 1182 (2018) 340-351.
- [33] K. Esra, F. Mansfeld, An evaluation of the electrochemical frequency modulation (EFM) technique, *Corros. Sci.* 48(4) (2006) 965-979.
- [34] I.B. Obot, I.B. Onyeachu, Electrochemical frequency modulation (EFM) technique: Theory and recent practical applications in corrosion research, *J. Mol. Liq.* 249 (2018) 83-96.
- [35] I.B. Onyeachu, D.S. Chauhan, K. Ansari, I.B. Obot, M.A. Quraishi, A.H. Alamri, Hexamethylene-1,6-bis(N-D-glucopyranosylamine) as a novel corrosion inhibitor for oil and gas industry: electrochemical and computational analysis, *New J. Chem.* 43 (2019) 7282-7293.
- [36] K.F. Khaled, Application of electrochemical frequency modulation for monitoring corrosion and corrosion inhibition of iron by some indole derivatives in molar hydrochloric acid, *Mater. Chem. Phys.* 112 (2008) 290-300.
- [37] D.q. Zhang, L.x. Gao, G.d. Zhou, Inhibition of copper corrosion by bis-(1-benzotriazolymethylene)-(2,5-thiadiazoly)-disulfide in chloride media, *Appl. Surf. Sci.* 225 (2004) 287-294.
- [38] H. Lgaz, F. El-hajjaji, M.E. Belghiti, B. Hammouti, S. Jodeh, O. Hamed, R. Salghi, Adsorption and Corrosion Inhibition Effect of 2-Mercaptobenzimidazole (Surfactant) on a Carbon Steel Surface in an Acidic Medium: Experimental and Monte Carlo Simulations, *Port. Electrochimica Acta* 36(3) (2018) 197-212.
- [39] Z.Z. Wang, Y.Y. Li, G.A. Zhang, Inhibitive effects of inhibitors on the galvanic corrosion between N80 carbon steel and 13Cr stainless steel under dynamic supercritical CO₂ conditions, *Corros. Sci.* 146(1) (2019) 121-133.
- [40] D. Kumar, V. Jain, B. Rai, Unravelling the Mechanisms of Corrosion Inhibition of Iron by Henna Extract: A Density Functional Theory Study, *Corros. Sci.* 142(1) (2018) 102-109.
- [41] K.M. Zohdy, A.M. El-Shamy, A. Kalmouch, E.A.M. Gad, The corrosion inhibition of (2Z,2'Z)-4,4'-(1,2-phenylene bis(azanediyl))bis(4-oxobut-2-enoic acid) for carbon steel in acidic media using DFT, *Egypt. J. Pet.* 28(4) (2019) 355-359.
- [42] A. Al-Amiery, F. Kassim, A. Kadhum, A.B. Mohamad, Synthesis and characterization of a novel eco-friendly corrosion inhibition for mild steel in 1 M hydrochloric acid, *Sci. Rep.* 6(1) (2016) 19890.
- [43] C. Tian Ser, P. Žuvela, M. Wah Wong, Prediction of corrosion inhibition efficiency of pyridines and quinolines on an iron surface using machine learning-powered quantitative structure property relationships, *Appl. Surf. Sci.* 512 (2020) 145612.
- [44] J. Haque, K.R. Ansari, V. Srivastava, M.A. Quraishi, I.B. Obot, Pyrimidine derivatives as novel acidizing corrosion inhibitors for N80 steel

- useful for petroleum industry: a combined experimental and theoretical approach, *J Ind Eng Chem* 49 (2017) 176-188.
- [45] M. Ramezanzadeh, G. Bahlakeh, Z. Sanaei, B. Ramezanzadeh, Corrosion inhibition of mild steel in 1 M HCl solution by ethanolic extract of eco-friendly *Mangifera indica* (mango) leaves: Electrochemical, molecular dynamics, Monte Carlo and ab initio study, *Appl. Surf. Sci.* 463(1) (2019) 1058-1077.
- [46] M. Rbaa, F. Benhiba, I.B. Obot, H. Oudda, I. Warad, B. Lakhri, A. Zarrouk, Two new 8-hydroxyquinoline derivatives as an efficient corrosion inhibitors for mild steel in hydrochloric acid: Synthesis, electrochemical, surface morphological, UV-visible and theoretical studies, *J. Mol. Liq.* 276 (2019) 120-133.
- [47] N. Obi-Egbedi, I. Obot, M. El-Khaiary, S. Umoren, E. Ebenso, Computational Simulation and Statistical Analysis on the Relationship Between Corrosion Inhibition Efficiency and Molecular Structure of Some Phenanthroline Derivatives on Mild Steel Surface, *Int. J. Electrochem. Sci.* 6(1) (2011) 5649-5675.
- [48] R.G. Parr, W. Yang, Density functional approach to the frontier-electron theory of chemical reactivity, *J. Am. Chem. Soc.* 106(14) (1984) 4049-4050.
- [49] A. Khadiri, R. Saddik, K. Bekkouche, A. Aouniti, B. Hammouti, N. Benchat, M. Bouachrine, R. Solmaz, Gravimetric, electrochemical and quantum chemical studies of some pyridazine derivatives as corrosion inhibitors for mild steel in 1 M HCl solution, *J Taiwan Inst Chem Eng* 58 (2016) 552-564.
- [50] C. Morell, A. Grand, A. Toro-Labbé, New dual descriptor for chemical reactivity *J. Phys. Chem.* 109 (2005) 205-112.
- [51] C. Morell, A. Grand, A. Toro-Labbe, Theoretical support for using the $\chi^2(r)$ descriptor *Chem. Phys. Lett.* 6(4) (2006) 425-342.
- [52] K.F. Khaled, Monte Carlo simulations of corrosion inhibition of mild steel in 0.5 M sulphuric acid by some green corrosion inhibitors, *J. Solid State Electrochem* 13 (2009) 1743-1756.
- [53] S. Kaya, B. Tüzün, C. Kay, I.B. Obot, determination of corrosion inhibition effects of amino acids: Quantum chemical and molecular dynamic simulation study. , *J Taiwan Inst Chem Eng* 58 (2016) 528-534.
- [54] I.B. Obot , S.A. Umoren, Z.M. Gasem, R. Suleiman, B. El Ali, Theoretical prediction and electrochemical evaluation of vinylimidazole and allylimidazole as corrosion inhibitors for mild steel in 1M HCl *J. Ind. Eng. Chem.* 21 (2015) 1328-1339.
- [55] T. Jianhong, G. Lei, *Int. J. Electrochem. Sci.* 10 (2015) 823-837.
- [56] M. El Faydy, F. Benhiba, A. Berisha, Y. Kerroum, C. Jama, B. Lakhri, A. Guenbour, I. Warad, A. Zarrouk, An experimental-coupled empirical investigation on the corrosion inhibitory action of 7-alkyl-8-Hydroxyquinolines on C35E steel in HCl electrolyte, *J. Mol. Liq.* 317 (2020) 113793.
- [57] Y.P. Khodyrev, E.S. Batyeva, E.K. Badeeva, E.V. Platova, L. Tiwari, O.G. Sinyashin, The inhibition action of ammonium salts of O,O- dialkyl dithiophosphoric acid on carbon dioxide corrosion of mild steel, *Corros. Sci.* 53(1) (2011) 976-983.
- [58] S.A. Ali, M.T. Saeed, S.U. Rahman, The isoxazolidines :a new class of corrosion inhibitors of mild steel in acidic medium, *Corros. Sci.* 45(2) (2003) 253-266.
- [59] M. Elayyachy, A. El Idrissi, B. Hammoutia, New thio-compounds as corrosion inhibitor for steel in 1M HCl, *Corros. Sci.* 48 (9) (2006) 2470-2479.
- [60] H. Keles, M. Keles, I. Dehri, O. Serindağ, The inhibitive effect of 6-amino-m-cresol and its Schiff base on the corrosion of mild steel in 0.5 M HCl medium, *Mater. Chem. Phys.* 112 (2008) 173-179.
- [61] M. Lebrini, F. Robert, H. Vezin, C. Roos, Electrochemical and quantum chemical studies of some indole derivatives as corrosion inhibitors for C38 steel in molar hydrochloric acid, *Corros. Sci.* 52(10) (2010) 3367-3376.
- [62] E. Bayol, A. Gürten, M. Dursun, K. Kayakirilmaz, Adsorption Behavior and Inhibition Corrosion Effect of Sodium Carboxymethyl Cellulose on Mild Steel in Acidic Medium, *ACTA PHYS-CHIM SIN.* 24(12) (2008) 2236-2243.
- [63] N. Belarbi, F. Dergal, I. Chikhi, S. Merah, Study of anticorrosion activity of Algerian L. stoechas oil on C38 carbon steel in 1 M HCl medium, *Int. J. Ind. Chem.* 9(1) (2018) 115-125.
- [64] X. Li, S. Deng, H. Fu, Adsorption and inhibition effect of vanillin on cold rolled steel in 3.0 M H₃PO₄, *Prog. Org. Coat.* 67(4) (2010) 420-426.